Nanoscale

ARTICLE

Received 00th January 20xx,
Accepted 00th January 20xx
DOI: 10.1039/x0xx00000x
www.rsc.org/

Preferential S/Se occupation in anisotropic $ReS_{2(1-x)}Se_{2x}$ monolayer alloy

Wen Wen,[a, e] Junhao Lin,[b] Kazu Suenaga,*[b] Yuzheng Guo,*[c] Yiming Zhu,[a] Hung-Pin Hsu,[d] and Liming Xie*[a, e]

Band structure engineering of two-dimensional (2D) metal dichalcogenides (TMDs) is crucial for their light-mater interaction and optoelectronic applications. Alloying of different metal or chalcogen elements with different stoichiometry in TMDs provides a versatile and efficient approach for modulating the electronic structure and property of 2D materials. In 2D alloys, quantification of spatial distribution and local coordination of atoms facilitates the establishment of structure-property relationship at atomic scale. Here, we have imaged and analyzed the atomic configuration of sulfur and selenium atoms in anisotropic $ReS_{1.4}Se_{0.6}$ by scanning transmission electron microscopy (STEM). In Z-contrast images, we have realized the identification and quantification of Re, Se and S at different coordination sites. Different from the random distribution of metal and chalcogen elements in $MoS_{2(1-x)}Se_{2x}$ and $Mo_{1-x}W_xS_2$, we find that Se atoms preferentially locate inside of Re4 diamonds in $ReS_{2(1-x)}Se_{2x}$. Further density function theory (DFT) calculations reveal electronic structure modulation for Se occupation at different sites.

Introduction

Atomically thin two-dimensional (2D) materials, including graphene, transition metal dichalcogenide monolayers and phosphorene, represent next-generation optoelectronic materials with advantages of mechanical flexibility, strong light-mater interaction and layer-dependent electronic structure.[1-8] High-performance field-effect transistors, light-emitting diodes, photodetectors and chemical sensors have been realized on single-component 2D materials and integrated Van der Waals heterostructures.[9-15] As a special category, 2D anisotropic crystals, such as phosphorene and ReX_2 (X= S, Se), possess low crystal lattice symmetry that endows them with anisotropic physical properties.[16,17] For example, polarization-dependent photoluminescence emission and Raman scattering,[18-20] anisotropic thermal and electronic conductivity,[21] intrinsic linear dichroism[22] have been demonstrated and led to device implementations toward anisotropic field-effect transistors,[13] thermoelectric devices[21] and polarization-sensitive photodetectors.[23]

Tailoring optoelectronic properties of anisotropic 2D materials is pivotal to their potential

[a]*CAS Key Laboratory of Standardization and Measurement for Nanotechnology, CAS Center for Excellence in Nanoscience, National Center for Nanoscience and Technology, Beijing 100190, P. R. China.*
E-mail: xielm@nanoctr.cn
[b]*National Institute of Advanced Industrial Science and Technology (AIST), Tsukuba 305-8565, Japan*
E-mail: suenaga-kazu@aist.go.jp
[c]*College of Engineering, Swansea University, Swansea, SA1 8EN, United Kingdom*
E-mail: yuzheng.guo@swansea.ac.uk
[d]*Department of Electronic Engineering, Ming Chi University of Technology, Taipei 243, Taiwan, Republic of China*
[e]*University of Chinese Academy of Sciences, Beijing 100049, People's Republic of China.*

applications.[24-30] Alloying of multi-component metal or chalcogen elements in TMDs provides an efficient approach for continuous tuning the bandgap of 2D materials. For example, Pan, Duan and their colleagues demonstrated that bandgap of CVD-grown $MoS_{2(1-x)}Se_{2x}$ can be continuously tuned from 1.856 eV of pure MoS_2 to 1.56 eV of $MoSe_2$ by controlling the S/Se atomic ratio.[31] Our group has carried out systematic investigation on the growth, bandgap, Raman spectra and electric transport of 2D alloys, including $MoS_{2(1-x)}Se_{2x}$, $Mo_{1-x}W_xSe$ and $ReS_{2(1-x)}Se_{2x}$.[32-35]

To further establish the structure-property relationship of 2D alloys, identification and quantification of elemental spatial distribution are prerequisite for understanding the local atomic coordination and physical properties. In previous reports, local coordination and elemental distribution of $Mo_{1-x}W_xS_2$ and $MoS_{2(1-x)}Se_{2x}$ have been characterized using aberration-corrected scanning transmission electron microscopy (STEM), displaying a randomly distributed of alloying atoms.[36-40] The random distribution of dopants in those alloys is derived from their intrinsic isotropic structure with high lattice symmetry. Compared to 2D materials with high lattice symmetry, the $ReS_{2(1-x)}Se_{2x}$ alloys possess large lattice distortion, which might lead to preferential occupation of S and Se at different coordination sites and show impacts on the electronic structure of alloys.

Here, we have employed STEM characterizations for directly mapping the atomic distributions of Re, Se and S in $ReS_{1.4}Se_{0.6}$ monolayers. The annular dark-field (ADF) images with Z contrast permit identifying the Re, Se and S atoms. In $ReS_{1.4}Se_{0.6}$, Re atomic chains with diamond-shaped Re4 clusters are formed. Various atomic coordination structures and the quantification of atomic occupation at different sites were realized by analyzing the STEM images. Different from the previous reported results of $Mo_{1-x}W_xS_2$ and $MoS_{2(1-x)}Se_{2x}$ with randomly distributed alloying atoms, the distribution of S and Se atoms shows an obvious difference at different coordination sites. Further DFT calculations evaluated the energy for substitution of S with Se at different sites, which is well consistent with the experimental results. According to the calculations, the different coordination structures also show different electronic bandgap.

Experimental

Preparation of $ReS_{1.4}Se_{0.6}$ alloys. $ReS_{1.4}Se_{0.6}$ single-crystal bulks were synthesized by chemical-vapor transport method by reaction at 1030 ºC for 10 days in evacuated quartz ampoules.[41] The stoichiometric mixture of elements (Re, S, Se) was added into a quartz ampoule and evacuated to a pressure of 10^{-6} Torr and sealed. Br_2 was used as transport agent to carry the elements. The $ReS_{1.4}Se_{0.6}$ monolayers were prepared by mechanical exfoliation of the single crystals.

Characterizations. STEM characterization was performed on a JEOL 2100F TEM with double DELTA corrector operated at 60 kV. The convergent angle for illumination is about 35 mrad, with a collection detector angle ranging from 62 to 200 mrad. The STEM samples were prepared by transferring the exfoliated $ReS_{1.4}Se_{0.6}$ monolayer flakes onto quantifoil TEM grids by an isopropanol-assisted direct transfer method.[42] The TEM grid was aligned with the monolayer region. A small droplet of isopropyl alcohol (IPA) was then dropped to the TEM grid and wait until dried. The SiO_2/Si substrate was then etched away by HF solvent, leaving the free-standing monolayer attached on the TEM grid.

DFT calculations. All calculations were performed with plane wave pseudo-potential code (CASTEP).[43] A 30 Å of vacuum is inserted between the monolayers to give an energy convergence of less than 0.01 eV. The structure is fully relaxed until the residual force is less than 0.02 eV/Å. The lattice constants are not fixed to allow fully relaxation at high doping concentrations. A 5×5 Monkhorst-Pack grid is used for reciprocal space integration of primitive cell. The default ultra-soft pseudo-potentials are used with cut-off energy of 500 eV. Different density functionals including local density approximation, PBE-style generalized gradient approximation, and screened exchange hybrid density functionals were tested to

Nanoscale

ARTICLE

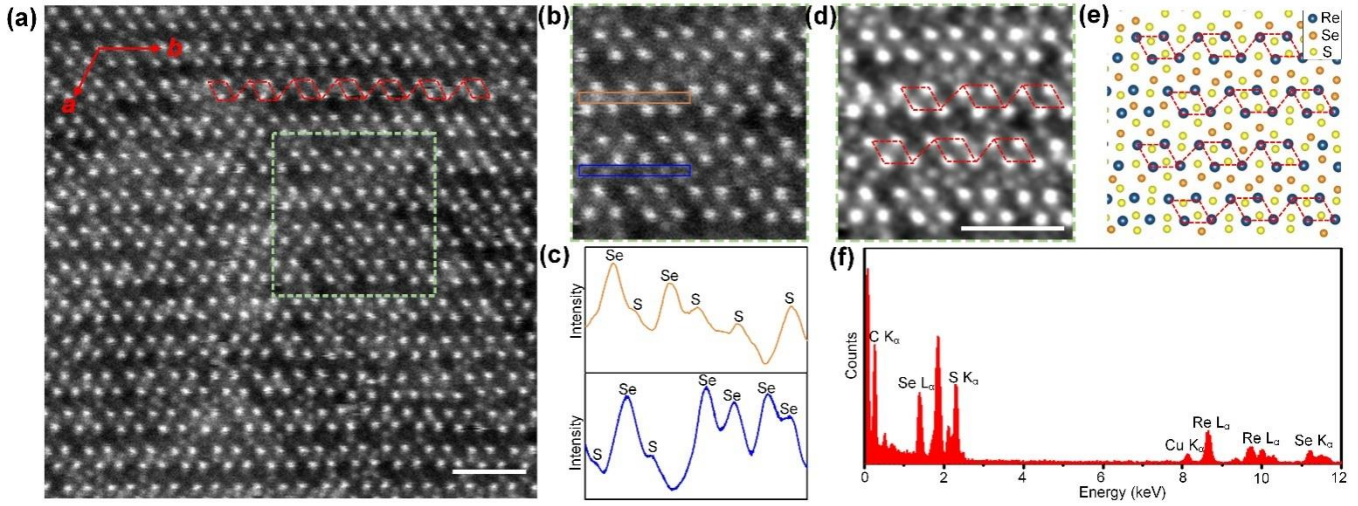

Fig. 1 STEM images and EDX analysis of $ReS_{1.4}Se_{0.6}$. (a) STEM and (b) zoom-in STEM images of $ReS_{1.4}Se_{0.6}$. (c) Intensity section along the lines marked in (b). (d) Filtered STEM image in (b), illustrating the spatial distribution of Re, S and Se atoms. (e) Scheme of atomic structure corresponding to the STEM image in (d). (f) EDX spectrum of the $ReS_{1.4}Se_{0.6}$monolayer.

give similar results (formation energy and band structure). The similar parameters were used as in our previous works on other 2D materials.[44, 45] The screened exchange hybrid functional[46] results are presented in the paper. The screened exchange hybrid functional mixes a Thomas-Fermi screened Hartree-Fock exchange into the local-density approximation (LDA), thus improving the accuracy of band structure calculations.[46] The van der Waals interaction was included empirically as in TS scheme.[47]

Results and discussion

Typical ReX_2 (X=S, Se) crystals are consisted by two buckled chalcogen-atom layers and an intercalated rhenium layer with zigzag atomic chains arising from Peierls distortion of the 1T structure. A representative STEM image of $ReS_{1.4}Se_{0.6}$ monolayer is shown in Fig. 1(a). The brightest spots are Re atoms, while the less bright spots are Se atoms. In our case, S atoms are slightly visible due to its smaller atomic number. Re atoms in $ReS_{1.4}Se_{0.6}$ are organized into one-dimensional (1D) zigzag atomic chains, which is consistent with the distorted 1T structure of ReS_2 and $ReSe_2$. Typical ReX_2 (X=S, Se) crystals are consisted by two buckled chalcogen-atom layers and an intercalated rhenium layer with zigzag atomic chains arising from Peierls distortion of the 1T structure. The Re chains constructed by diamond-shaped Re4 clusters (marked by red line in Fig 1(a)) is defined as direction of *b* axis, while *a* axis is *ca.* 119.8° from *b* axis. The composition of $ReS_{1.4}Se_{0.6}$ alloy was further validated by energy dispersive X-ray spectrum (EDS) analysis. As shown in Fig. 1(f), the peaks at 1.38, 2.31, 8.65 and 11.22 keV can be assigned to Se L_α, S K_α, Re L_α and Se K_α bands, respectively, which confirms the elemental composition of $ReS_{1.4}Se_{0.6}$ monolayer. The atomic ratio of S/Se is determined to be 70/30, which is well consistent with the predesigned stoichiometry in the growth of single crystals.

To analyze the local atomic coordination structure of $ReS_{1.4}Se_{0.6}$, a zoom-in STEM image is shown in Fig. 1(b, d) and the corresponding atomic structure is shown in Fig. 1(e). S and Se sites located in and between the Re atomic chains are

Nanoscale

ARTICLE

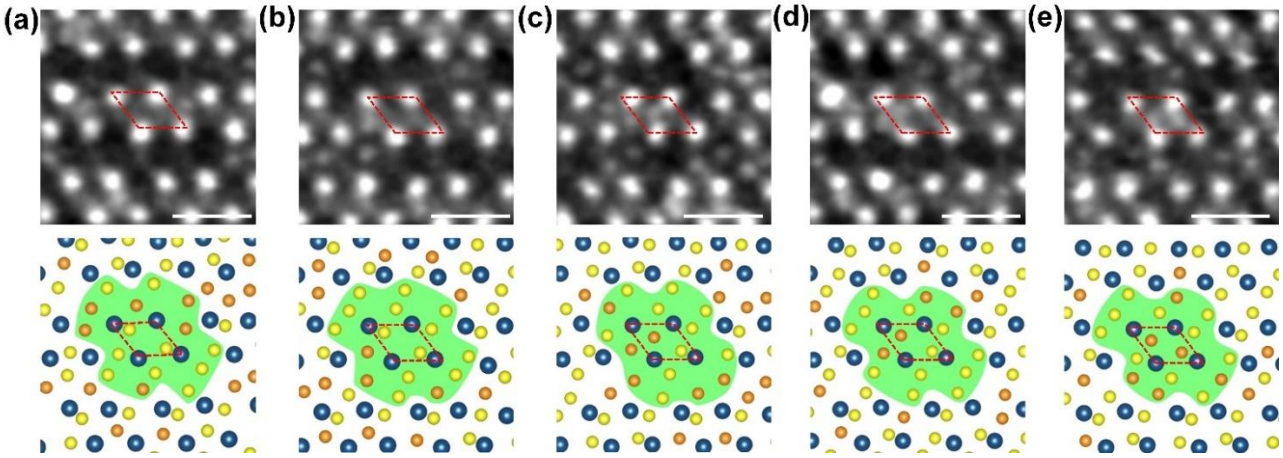

Fig. 2 STEM images and the corresponding atomic structures of $ReS_{1.4}Se_{0.6}$. (a-e) Representative STEM images (top) and corresponding atomic structures (bottom). The green color marks S and Se atoms coordinated around the Re4 clusters.

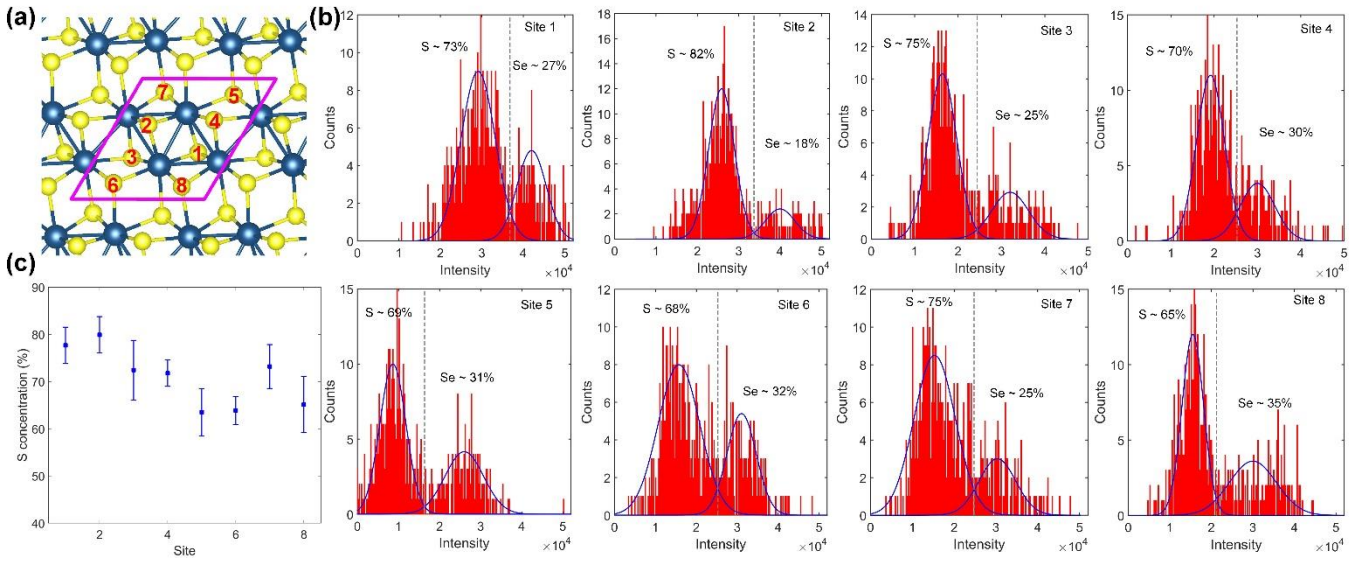

Fig. 3 Quantitative analysis of atomic distributions of S and Se. (a) A Scheme of ReX_2 (X=S, Se) structure with eight different coordinate sites in a unit cell. (b) Statistics of S and Se from STEM images for each coordinate site marked in (a). (c) Percentage of Se at different sites.

marked as orange and blue regimes in Fig. 1(b). Fig. 1(c) depicts the section profile along the orange and blue lines, indicating different STEM intensity for S and Se atoms. In this regime, Se atoms preferentially occupy the sites between two Re atomic chains (marked as blue), while the sites located in the Re4 chains (marked as orange) possess low Se density. According to the STEM result in Fig. 1(a), the local atomic coordination structure in $ReS_{2(1-x)}Se_{2x}$ alloys is analyzed based on the coordinated chalcogen atoms around the diamond-shaped Re4 units.

Fig. 2 shows typical STEM images of several alloyed regions and schemes of the corresponding atomic coordination structure. As shown in those schemes, each Re atom is coordinated with 6 S/Se

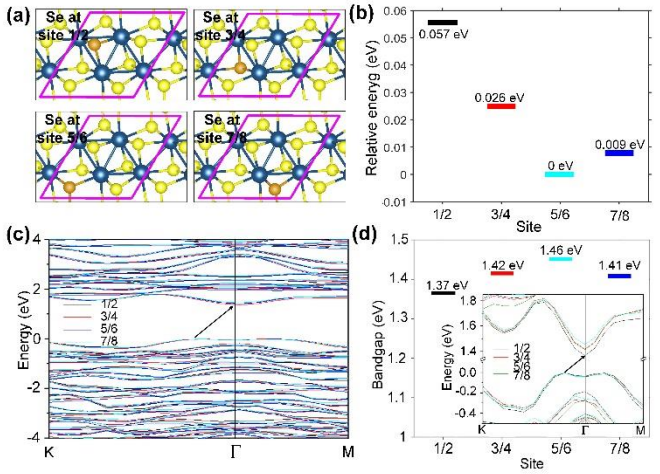

Fig. 4 DFT calculations of $ReS_{2(1-x)}Se_{2x}$ alloys. (a) Scheme of Se substitution of S at different sites. (b) Energy for Se substitution of S. (c) Electron band structure and (d) bandgaps of $ReS_{2(1-x)}Se_{2x}$ with Se coordination at different sites. Inset of 4(d) indicates the magnified electronic band structure at valence band maximum and conduction band minimum.

atoms and total 16 coordinated S/Se atoms in the Re4 unit, which is marked by a green shade in the scheme. The distribution of Se and S atoms at different coordination sites can be extracted from STEM images. Representative STEM images shown in Fig. S1 illustrate S/Se coordination along Re4 atomic chains. S and Se atoms can be observed in and between the Re atomic chains.

To further quantify the distribution of S and Se atoms in $ReS_{1.4}Se_{0.6}$, we performed a statistical analysis on the distribution of the S/Se atoms at various alloyed sites within a larger region. Different S/Se sites with different bonding conditions in the Re4 unit cell is marked with site numbers of 1 to 8 in Fig. 3(a). The data analysis was carried out using custom-written Matlab (MathWorks) code for extracting the S/Se concentration at different coordination sites (Details shown in Supporting Note S1, Fig. S2, S3). Note that the low-intensity vacancies could be counted as S atoms in our analysis, but the low vacancy concentration in high-quality 2D crystals leads to the limited impacts on the accuracy of quantity of S and Se atoms at different sites[48-50]. The statistic result of a representative region is shown in Fig. 3(b). Since the intensity is directly related to the atomic number of the atomic specie, the number of S and Se occupations can be approximately separated in the intensity distribution for each site (Fig. 3b). The identification of S and Se was performed by fitting the intensity profile of different coordination sites with two individual Gaussian distribution. To obtain the S and Se coordination structure in $ReS_{1.4}Se_{0.6}$, we performed analysis on 5 different STEM images captured at different samples. The statistical results are shown in Fig. 3(c). For site 1-8, S and Se percentages are about (78%, 22%), (80%, 20%), (72%, 28%), (72%, 28%), (64%, 36%), (64%, 36%), (73%, 27%) and (65%, 35%). Note that sites 1/2 possess obviously higher percentages of S atoms while sites 5/6 possess obviously higher percentages of Se atoms.

To gain further insights into the alloying behavior of $ReS_{1.4}Se_{0.6}$, we carried out DFT calculations on stability and electronic structure of different Se/S coordination configurations. Owing to the inversion symmetry in the $ReS_{1.4}Se_{0.6}$, eight different sites marked in Fig. 3(a) can be categorized as 4 sets (Fig. 4(a)). That is, Se atoms substitution of S atoms at sites of 1/2, 3/4, 5/6, and 7/8. We chose the site with minimum energy for Se substitution, site 5/6, to be the reference state (0 eV) (Fig. 4(b)). The energy of each site is defined as the energy difference between each site and site 5/6. The 5/6 site has the largest volume compared due to the asymmetry geometry of ReS_2 cell so that it is easier to accommodate the larger Se atom. This is consistent with observed lowest S occupation (i.e., highest Se occupation) in STEM images. Higher energy is needed for Se substitution at other sites, for example, 57, 26, 9 meV for substitution sites of 1/2, 3/4 and 7/8, respectively (Fig. 4(b)). According to the DFT-calculated energy, we further calculated the Se relative occupation probability and percentage at each sites at the growth temperature of 1303 K (Detailed methods shown in Supporting Note S2). The calculated Se percentages at different coordination sites match well with the experimental results (further comparison in the Table S1).

Band structure of ReS1.4Se0.6 alloys with different local atomic coordination was further calculated. Representative electronic band structure with Se substitution at sites 1/2, 3/4, 5/6, and 7/ 8 are shown in Fig. 4(c) and 4(d) inset. $ReS_{1.4}Se_{0.6}$ alloys with different atomic coordination possess similar indirect bandgap. For Se substitution at 1/2, 3/4, 5/6 and 7/8 sites, the bandgap are calculated to be 1.37,

1.42, 1.46, 1.41 eV, respectively (Fig. 4(d)). This suggests that preferential occupation of Se at sites 5/6 leads to a slightly higher bandgap. Preferential occupation of one component has been observed in other alloys and leads to the property engineering different from perfect random alloys.[51-53] Due to anisotropic nature of the X site in ReX2, other doping elements other than S/Se, such as Te, O and so on, are also expected to have preferred occupations and new properties can be expected.

Conclusions

Different from randomly distribution of alloying elements in the $Mo_{1-x}W_xS_2$ or $MoS_{2(1-x)}Se_{2x}$, Se atoms preferentially occupy the sites located between Re chains in anisotropic $ReS_{1.4}Se_{0.6}$ from STEM imaging and DFT calculation. Owing to the low-symmetry structure of $ReS_{2(1-x)}Se_{2x}$ alloys and hence unequivalent S/Se sites, preferential S/Se occupations have an effect on the electronic bandgaps. This work provides fundamental understanding the atomic structure and electronic structure on anisotropic 2D $ReS_{2(1-x)}Se_{2x}$ materials.

Acknowledgements

The authors acknowledge support from NSFC (21373066, 21673058, 11474277, 11434010, and 11225421), Beijing Nova programme (Z151100000315081), Beijing Talents Fund (2015000021223ZK17), Strategic Priority Research Program of CAS (XDA09040300), HPC Wales (HPCW0285) and Key Research Program of Frontier Sciences of CAS (QYZDB-SSW-SYS031). J.L. and K.S. acknowledge JST-ACCEL and JSPS KAKENHI (JP16H06333 and P16823) for financial support.

References

1. G. Fiori, F. Bonaccorso, G. Iannaccone, T. Palacios, D. Neumaier, A. Seabaugh, S. K. Banerjee and L. Colombo, *Nat. Nanotechnol.*, 2014, 9, 768-779.
2. D. Jariwala, T. J. Marks and M. C. Hersam, *Nat. Mater.*, 2017, 16, 170-181.
3. F. Xia, H. Wang, D. Xiao, M. Dubey and A. Ramasubramaniam, *Nat. Photon.*, 2014, 8, 899-907.
4. Q. H. Wang, K. Kalantar-Zadeh, A. Kis, J. N. Coleman and M. S. Strano, *Nat. Nanotechnol.*, 2012, 7, 699-712.
5. O. V. Yazyev and Y. P. Chen, *Nat. Nanotechnol.*, 2014, 9, 755-767.
6. F. Schwierz, *Nat. Nanotechnol.*, 2010, 5, 487-496.
7. A. K. Geim and I. V. Grigorieva, *Nature*, 2013, 499, 419-425.
8. X. Liu, T. Galfsky, Z. Sun, F. Xia, E.-c. Lin, Y.-H. Lee, S. Kéna-Cohen and V. M. Menon, *Nat. Photon.*, 2015, 9, 30-34.
9. F. H. L. Koppens, T. Mueller, P. Avouris, A. C. Ferrari, M. S. Vitiello and M. Polini, *Nat. Nanotechnol.*, 2014, 9, 780-793.
10. F. Withers, O. Del Pozo-Zamudio, A. Mishchenko, A. P. Rooney, A. Gholinia, K. Watanabe, T. Taniguchi, S. J. Haigh, A. K. Geim, A. I. Tartakovskii and K. S. Novoselov, *Nat. Mater.*, 2015, 14, 301-306.
11. R. Kappera, D. Voiry, S. E. Yalcin, B. Branch, G. Gupta, A. D. Mohite and M. Chhowalla, *Nat. Mater.*, 2014, 13, 1128-1134.
12. B. Radisavljevic and A. Kis, *Nat. Mater.*, 2013, 12, 815-820.
13. L. Li, Y. Yu, G. J. Ye, Q. Ge, X. Ou, H. Wu, D. Feng, X. H. Chen and Y. Zhang, *Nat. Nanotechnol.*, 2014, 9, 372-377.
14. M. Zhao, Y. Ye, Y. Han, Y. Xia, H. Zhu, S. Wang, Y. Wang, D. A. Muller and X. Zhang, *Nat. Nanotechnol.*, 2016, 11, 954-959.
15. A. A. Balandin, *Nat. Nanotechnol.*, 2013, 8, 549-555.
16. X. Wang, A. M. Jones, K. L. Seyler, V. Tran, Y. Jia, H. Zhao, H. Wang, L. Yang, X. Xu and F. Xia, *Nat. Nanotechnol.*, 2015, 10, 517-521.
17.D. Çakır, C. Sevik and F. M. Peeters, *Phys. Rev. B*, 2015, 92, 165406.
18. X. Zhang, Q.-H.Tan, J.-B.Wu, W. Shi and P.-H. Tan, *Nanoscale*, 2016, 8, 6435-6450.
19. H. Zhao, J. Wu, H. Zhong, Q. Guo, X. Wang, F. Xia, L. Yang, P. Tan and H. Wang, *Nano Res.*, 2015, 8, 3651-3661.
20.R. Xu, S. Zhang, F. Wang, J. Yang, Z. Wang, J. Pei, Y. W. Myint, B. Xing, Z. Yu, L. Fu, Q. Qin and Y. Lu, *ACS Nano*, 2016, 10, 2046-2053.
21. S. Lee, F. Yang, J. Suh, S. Yang, Y. Lee, G. Li, H. Sung Choe, A. Suslu, Y. Chen, C. Ko, J. Park, K. Liu, J. Li, K. Hippalgaonkar, J. J. Urban, S. Tongay and J. Wu, *Nat. Commun.*, 2015, 6, 8573.
22.J. Qiao, X. Kong, Z.-X. Hu, F. Yang and W. Ji, *Nat. Commun.*, 2014, 5, 4475.
23.H. Yuan, X. Liu, F. Afshinmanesh, W. Li, G. Xu,

J. Sun, B. Lian, A. G. Curto, G. Ye, Y. Hikita, Z. Shen, S.-C. Zhang, X. Chen, M. Brongersma, H. Y. Hwang and Y. Cui, *Nat. Nanotechnol.*, 2015, 10, 707-713.
24. D. Voiry, A. Goswami, R. Kappera, e. SilvaCecilia de Carvalho Castro, D. Kaplan, T. Fujita, M. Chen, T. Asefa and M. Chhowalla, *Nat. Chem.*, 2015, 7, 45-49.
25. Z. Yu, Y. Pan, Y. Shen, Z. Wang, Z.-Y.Ong, T. Xu, R. Xin, L. Pan, B. Wang, L. Sun, J. Wang, G. Zhang, Y. W. Zhang, Y. Shi and X. Wang, *Nat. Commun.*, 2014, 5, 5290.
26. S. S. Chou, M. De, J. Kim, S. Byun, C. Dykstra, J. Yu, J. Huang and V. P. Dravid, *J. Am. Chem. Soc.*, 2013, 135, 4584-4587.
27. S. Lei, X. Wang, B. Li, J. Kang, Y. He, A. George, L. Ge, Y. Gong, P. Dong, Z. Jin, G. Brunetto, W. Chen, Z.-T. Lin, R. Baines, D. S. Galvão, J. Lou, E. Barrera, K. Banerjee, R. Vajtai and P. Ajayan, *Nat. Nanotechnol.*, 2016, 11, 465-471.
28. M. Amani, D.-H. Lien, D. Kiriya, J. Xiao, A. Azcatl, J. Noh, S. R. Madhvapathy, R. Addou, S. KC, M. Dubey, K. Cho, R. M. Wallace, S.-C. Lee, J.-H. He, J. W. Ager, X. Zhang, E. Yablonovitch and A. Javey, *Science*, 2015, 350, 1065-1068.
29. D. Kiriya, M. Tosun, P. Zhao, J. S. Kang and A. Javey, *J. Am. Chem. Soc.*, 2014, 136, 7853-7856.
30. Y. Zhang, Y. Wen, Y. Liu, D. Li and J. Li, *Electrochem. Commun.*, 2004, 6, 1180-1184.
31. H. Li, X. Duan, X. Wu, X. Zhuang, H. Zhou, Q. Zhang, X. Zhu, W. Hu, P. Ren, P. Guo, L. Ma, X. Fan, X. Wang, J. Xu, A. Pan and X. Duan, *J. Am. Chem. Soc.*, 2014, 136, 3756-3759.
32. Q. Feng, Y. Zhu, J. Hong, M. Zhang, W. Duan, N. Mao, J. Wu, H. Xu, F. Dong, F. Lin, C. Jin, C. Wang, J. Zhang and L. Xie, *Adv. Mater.*, 2014, 26, 2648-2653.
33. M. Zhang, J. Wu, Y. Zhu, D. O. Dumcenco, J. Hong, N. Mao, S. Deng, Y. Chen, Y. Yang, C. Jin, S. H. Chaki, Y.-S. Huang, J. Zhang and L. Xie, *ACS Nano*, 2014, 8, 7130-7137.
34. Y. Chen, J. Xi, D. O. Dumcenco, Z. Liu, K. Suenaga, D. Wang, Z. Shuai, Y.-S. Huang and L. Xie, *ACS Nano*, 2013, 7, 4610-4616.
35. W. Wen, Y. Zhu, X. Liu, H.-P.Hsu, Z. Fei, Y. Chen, X. Wang, M. Zhang, K.-H.Lin, F.-S.Huang, Y.-P.Wang, Y.-S.Huang, C.-H. Ho, P.-H. Tan, C. Jin and L. Xie, *Small*, 2017, 13, 1603788.
36. Y.-C. Lin, H.-P.Komsa, C.-H.Yeh, T. Björkman, Z.-Y.Liang, C.-H. Ho, Y.-S. Huang, P.-W. Chiu, A. V. Krasheninnikov and K. Suenaga, *ACS Nano*, 2015, 9, 11249-11257.
37. Y.-C. Lin, D. O. Dumcenco, Y.-S. Huang and K. Suenaga, *Nat. Nanotechnol.*, 2014, 9, 391-396.
38. M. H. Gass, U. Bangert, A. L. Bleloch, P. Wang, R. R. Nair and A. K. Geim, *Nat. Nanotechnol.*, 2008, 3, 676-681.
39. D. O. Dumcenco, H. Kobayashi, Z. Liu, Y.-S. Huang and K. Suenaga, *Nat. Commun.*, 2013, 4, 1351.
40. Y. Gong, Z. Liu, A. R. Lupini, G. Shi, J. Lin, S. Najmaei, Z. Lin, A. L. Elías, A. Berkdemir, G. You, H. Terrones, M. Terrones, R. Vajtai, S. T. Pantelides, S. J. Pennycook, J. Lou, W. Zhou and P. M. Ajayan, *Nano Lett.*, 2014, 14, 442-449.
41.C.H. Ho, Y.S. Huang, P.C. Liao, K.K. Tiong, *J. Phys. Chem. Sol.* 1999, 60, 1797.
42. D. Pacilé, J. C. Meyer, Ç. Ö. Girit and A. Zettl, *Appl. Phys. Lett.*, 2008, 92, 133107.
43.S. J. Clark, M. D. Segall, C. J. Pickard, P. J. Hasnip, M. I. Probert, K. Refson and M. C. Payne, *Z. Krist.-Cryst. Mater.*, 2005, 220, 567-570.
44. D. Liu, Y. Guo, L. Fang and J. Robertson, *Appl. Phys. Lett.*, 2013, 103, 183113.
45.Y. Guo and J. Robertson, *Appl. Phys. Lett.*, 2016, 108, 233104.
46. S. J. Clark and J. Robertson, *Phys. Rev. B*, 2010, 82, 085208.
47. A. Tkatchenko and M. Scheffler, *Phys. Rev. Lett.*, 2009, 102, 073005.
48. H. Qiu, T. Xu, Z. Wang, W. Ren, H. Nan, Z. Ni, Q. Chen, S. Yuan, F. Miao, F. Song, G. Long, Y. Shi, L. Sun, J. Wang and X. Wang, *Nat. Commun.*, 2013, 4, 2642.
49. J. Hong, Z. Hu, M. Probert, K. Li, D. Lv, X. Yang, L. Gu, N. Mao, Q. Feng, L. Xie, J. Zhang, D. Wu, Z. Zhang, C. Jin, W. Ji, X. Zhang, J. Yuan and Z. Zhang, *Nat. Commun.*, 2015, 6, 6293.
50. W. M. Parkin, A. Balan, L. Liang, P. M. Das, M. Lamparski, C. H. Naylor, J. A. Rodríguez-Manzo, A. T. C. Johnson, V. Meunier and M. Drndić, *ACS Nano*, 2016, 10, 4134-4142.
51. X. He, X. Liu, C. You, Y. Zhang, R. Li and R. Yu, *J. Mater. Chem. C*, 2016, 4, 10691-10700.
52. Q. Zhang, B. Zhao, M. Fang, C. Liu, Q. Hu, F. Fang, D. Sun, L. Ouyang and M. Zhu, *Inorg. Chem.*, 2012, 51, 2976-2983.
53. X. Hou, S. Chen, Z. Du, X. Liu and J. Cui, *RSC*

Adv., 2015, 5, 102856-102862.